Hindawi
Journal of Robotics
Volume 2021, Article ID 9979713, 14 pages
https://doi.org/10.1155/2021/9979713

Research Article

A Fixed-Time Hierarchical Formation Control Strategy for Multiquadrotors

Miaojie Huang and Qiang Lu

School of Automation, Hangzhou Dianzi University, Hangzhou, China

Correspondence should be addressed to Miaojie Huang; hmj882@hdu.edu.cn

Received 16 March 2021; Revised 8 April 2021; Accepted 23 April 2021; Published 6 May 2021

Academic Editor: Yaoyao Wang

This paper deals with the problem of multiquadrotor collaborative control by developing and analyzing a new type of fixed-time formation control algorithm. The control strategy proposes a hierarchical control framework, which consists of two layers: a coordinating control layer and a tracking control layer. On the coordinating control layer, according to the fixed-time consistency theory, the virtual position and virtual velocity of each quadrotor are calculated and acquired to form a virtual formation, and the virtual velocity reaches consistency. On the tracking control layer, the real position and the real velocity track the virtual position and the virtual velocity, respectively. Thus, multiquadrotor can achieve the required formation shape and velocity consensus. Finally, the comparative simulations are carried out to illustrate the feasibility and superiority of the proposed fixed-time hierarchical formation control method for multiquadrotor collaborative control.

1. Introduction

Multiquadrotor systems have been widely used in various fields in the last decade, for example, agricultural plant protection, expressing, aerial photogrammetry, and emergency relief [1–6]. Compared with a single quadrotor, the advantages of multiquadrotor collaborative work mainly come from the two aspects, information fusion and resource complementation. In the process of executing tasks by multiple quadrotors, even if a single quadrotor fails, it will not cause the failure of the entire mission, which can greatly improve the reliability and fault tolerance of the system, so that it can satisfy the requirements of task time, space, and optimization. However, from the cybernetic perspective, the control of multiquadrotors will be more challenging and difficult, because not only the flight status of the single quadrotor but also the cooperative control between multiple quadrotors is considered. Therefore, how to solve the convergence problem of multiple quadrotors and how to increase the convergence rate are the hot topics for current research in cooperative control of multiquadrotor system.

Up to now, researchers have achieved rich research results in the field of cooperative control of multiagents and have put forward many theories of formation control, which include leader-follower methods, virtual structure methods, and behavior-based methods and all of these are widely used in the field of multiquadrotor formation control. By adopting the lead-following formation architecture, the formation control methods which combined state estimation and backstepping method were given in [7]. In [8], a behavior-based decentralized method for robust formation flight control technology for multiple UAVs is proposed. A behavior-based formation flight control method is designed in [9]; it solves the thorny problem that traditional formation flying control based on virtual architecture has a heavier burden on data communication; this theory can enhance the obstacle avoidance and risk avoidance capabilities of UAVs in unknown environments and can provide ideas for aircraft in low-altitude coordinated operations. Furthermore, in order to overcome the difficulties that most of the results of collaborative formation control are asymptotically stable, the finite-time consensus method is proposed and widely used in the field of multiagents [10, 11];

the strategy of finite-time control introduced in [12] can ensure that the closed-loop system improves the response characteristics of the system and it is finite-time convergence. Moreover, an optimized new finite-time control strategy given in [13] can provide better disturbance rejection performance. In [14], this paper introduced that the finite-time consensus algorithm was used to construct the position dynamics model and attitude dynamics model, respectively, so that multiquadrotors can achieve the desired formation shape. However, the finite-time consistency algorithm has certain flaws, and its convergence time is also affected by the initial state information. Therefore, researchers have made improvements on the basis of finite-time stability; the fixed-time consistency theory has emerged as the times require.

Compared with the finite-time control theory, fixed-time consistency has better convergence and robustness. In [15], Polyakov proposed the concept of fixed-time consistency on the basis of finite-time stability. For uncertain linear objects, two new nonlinear control algorithms are proposed, which allowed the system trajectory to be adjusted independently under initial conditions to ensure the convergence time. The convergence time will not be affected by the system's initial state. In [16], an edge-based distributed optimization method for multirobot system is proposed, which guaranteed reaching consistency at a fixed time. In [17], aiming at the leader-follower multiagent consistency problem, a fixed-time consistency convergence protocol is proposed to ensure that multiagents converge quickly within a set time. In [18], a fixed-time fault-tolerant controller is designed to solve the problem of spacecraft rendezvous with thruster failure and external disturbance.

As far as the authors know, due to the strong nonlinear coupling and high dimension of multiquadrotor system, there are relatively few references for formation control of multiple quadrotors. For some complex control systems, new types of control methods are often needed. In [19], aiming at the problem that it is difficult to obtain velocity signal in electrohydraulic servomechanisms, a practical adaptive tracking controller is designed and the new kind of controller that can track the unknown parameter estimates only depends on the actual position and desired trajectory. In [20], for the complex hydraulic systems, a new time-delay model is proposed to approximate the valve dynamics and this model will not increase the order of the system. Therefore, for a highly complex multiquadrotor system, the main motivation of this paper is to establish a formation control algorithm.

The main contribution of this paper is to decouple the originally highly complex quadrotors formation control model and simplify it into two-layer structure. The upper layer designs a coordinating control layer based on a fixed-time method to calculate and get virtual state information of each quadrotor. The lower layer is the PID-based tracking control algorithm, which is used to obtain the real state information to track the virtual position and velocity. On the basis of the given architecture, the multiquadrotors will reach the desired formation and velocity consensus; moreover, the convergence efficiency is significantly improved.

2. Preliminaries

2.1. Communication Scheme. The communication topology structure among multiple quadrotors is denoted by using an undirected graph $G_n = \{V, E, A\}$, where it includes the adjacency matrix $A = [a_{ij}] \in \mathbb{R}^{n\times n}$, $i, j \in B$, where a_{ij} is the communication weight between the ith quadrotor and the jth quadrotor, when the aircraft i links to the aircraft j; then $a_{ij} > 0$. The set of nodes $V = \{v_1, v_2, \ldots, v_n\}$, E is an edge set ($e_{ij} \in E$), where e_{ij} is the communication link between the ith quadrotor and the jth quadrotor. $L_{G_n} = [l_{ij}] \in \mathbb{R}^{n\times n}$ is a Laplacian matrix of G_n. Let $G_{n+1} = G_n \cup v_0$ be an extended graph, where v_0 denotes a virtual leader. If the other quadrotors (follows) can get messages from the leader, $a_{i0} > 0\,(i = 1, \ldots, n)$; otherwise, $a_{i0} = 0$, let $M = \mathrm{diag}\{a_{10}, \ldots, a_{n0}\}$, which is true communication matrix.

2.2. Dynamics Model. In order to describe the position, attitude, velocity, and other information of the multiquadrotors in the spatial range, two coordinate systems were established, where one is geographic coordinate system $E(X_e, Y_e, Z_e)$ and the other is the body coordinate system $B(X_b, Y_b, Z_b)$. In particular, the body coordinate system can be transformed by the transformation rotation formula to a geographic coordinate system as follows:

$$R = \begin{bmatrix} c_{\psi_i}c_{\theta_i} & s_{\phi_i}s_{\theta_i}c_{\psi_i} - c_{\phi_i}s_{\psi_i} & c_{\phi_i}s_{\theta_i}c_{\psi_i} + s_{\phi_i}s_{\psi_i} \\ c_{\theta_i}s_{\psi_i} & s_{\phi_i}s_{\theta_i}s_{\psi_i} + c_{\phi_i}c_{\psi_i} & c_{\phi_i}s_{\theta_i}s_{\psi_i} - s_{\phi_i}c_{\psi_i} \\ -s_{\theta_i} & s_{\phi_i}c_{\theta_i} & c_{\phi_i}c_{\theta_i} \end{bmatrix}, \tag{1}$$

where s_{θ_i} and c_{θ_i} denote $\sin\ \theta_i$ and $\cos\ \theta_i$ ($i \in \Gamma = \{1, 2, \ldots, n\}$), respectively. Furthermore, it is usually required to use six degree-of-freedom variables to describe the operation of the quadrotor in three-dimensional space. The coordinates of each quadrotor are expressed as

$$(x_i, y_i, z_i, \phi_i, \theta_i, \psi_i)^T \in \mathbb{R}^6, \quad i \in 1, 2, \ldots, n, \tag{2}$$

where $r_i = [x_i, y_i, z_i]^T \in \mathbb{R}^3$ and $\Phi_i = [\phi_i, \theta_i, \psi_i]^T \in \mathbb{R}^3$ represent the Euler angles to denote the attitude of the quadrotor, which include the roll angle ϕ_i (rotation Euler angles around x-axis), the pitch angle θ_i (rotation Euler angles around y-axis), and the yaw angle ψ_i (rotation Euler angles around z-axis) [21].

2.2.1. Position Dynamics Model. Due to the fact that the aerodynamic effects cannot be neglected, the position dynamical model for each quadrotor is presented as follows:

$$\begin{aligned} \ddot{x}_i &= \frac{T_i}{m_i}\left(\cos\ \phi_i \sin\ \theta_i \cos\ \psi_i + \sin\ \psi_i \sin\ \phi_i\right) - \frac{k_{x,i}}{m_i}\dot{x}_i, \\ \ddot{y}_i &= \frac{T_i}{m_i}\left(\cos\ \phi_i \sin\ \theta_i \cos\ \psi_i + \sin\ \psi_i \sin\ \phi_i\right) - \frac{k_{x,i}}{m_i}\dot{x}_i, \\ \ddot{z}_i &= \frac{T_i}{m_i}\cos\ \phi_i \cos\ \theta_i - g - \frac{k_{z,i}}{m_i}\dot{z}_i, \\ i &\in \Gamma, \end{aligned} \tag{3}$$

where m_i is the mass of the quadrotor; $k_{x,i}$, $k_{y,i}$, and $k_{z,i}$ are the aerodynamic drag coefficients; and g represents the gravitational acceleration in geographic coordinate system.

2.2.2. Attitude Dynamics Model. From [22], the dynamics model of each quadrotor's attitude based on Euler angle is given as follows:

$$\begin{aligned}\ddot{\phi}_i &= \frac{\left(I_{y,i} - I_{z,i}\right)\dot{\theta}_i\dot{\psi}_i + \tau_{\phi,i} - k_{\phi,i}\dot{\phi}_i}{I_{x,i}},\\ \ddot{\theta}_i &= \frac{\left(I_{z,i} - I_{x,i}\right)\dot{\phi}_i\dot{\psi}_i + \tau_{\theta,i} - k_{\theta,i}\dot{\theta}_i}{I_{y,i}},\\ \ddot{\psi}_i &= \frac{\left(I_{x,i} - I_{y,i}\right)\dot{\theta}_i\dot{\phi}_i + \tau_{\psi,i} - k_{\psi,i}\dot{\psi}_i}{I_{z,i}},\\ i &\in \Gamma,\end{aligned} \tag{4}$$

where $k_{\phi,i}$, $k_{\theta,i}$, and $k_{\psi,i}$ represent the air resistance coefficients and $I_{x,i}$, $I_{y,i}$, and $I_{z,i}$ denote the moments of inertia, which are all constant.

2.3. Lemmas. In this section, in order to provide theoretical support for subsequent stability proof, we will introduce some lemmas about fixed-time method.

Lemma 1. *For a double integral system as shown in equation (2), if the controller meets the following conditions, it is called fixed time stability:*

$$\begin{aligned}\lim_{t\longrightarrow T}\left\|x_i(t) - x_j(t)\right\| + \left\|v_i(t) - v_j(t)\right\| &= 0,\\ \left\|x_i(t) - x_j(t)\right\| + \left\|v_i(t) - v_j(t)\right\| &= 0,\\ \forall t > T.\end{aligned} \tag{5}$$

Lemma 2 (see [15]). *If there exists a continuous radially unbounded function $F\colon \mathbb{R}^n \longrightarrow \mathbb{R}_+ \cup \{0\}$ meanwhile 1)$F(x) = 0 \Rightarrow x \in M$; 2) any solution $x(t)$ of (1) suffice the inequality $D^*F(x(t)) \le -(\alpha F^p(x(t)) + \beta F^q(x(t)))^k$ for $\alpha, \beta, p, q, k > 0$; $pk < 1, qk > 1$ so $M \subseteq R^n$ is globally fixed-time attractive for (1) and $T(x_0) \le (1/\alpha^k(1 - pk)) + (1/\beta^k(qk - 1))$, $\forall x_0 \in \mathbb{R}^n$.*

Lemma 3. *When $p_i \in R, i \in \Gamma$, and $0 < b \le 1$, mathematical relationship is presented as follows:*

$$\left(\sum_{i=1}^{n}\left|p_i\right|\right)^b \le \sum_{i=1}^{n}\left|p_i\right|^b \le n^{1-b}\left(\sum_{i=1}^{n}\left|p_i\right|\right)^b. \tag{6}$$

3. Hierarchical Formation Control Architecture

This section will introduce the core layered structure, shown in Figure 1; it will be divided into two parts to illustrate:

(1) For the coordinated control level, due to the fact that this layer of collaborative control algorithm is separated from the control of a single quadrotor, it belongs to model-free control. The virtual leader's state information can be used as input data, and the output data can be used as virtual state information, which are acquired by fixed-time consensus method. Next, we define the leader's position $r_0 = [x_0, y_0, z_0]^T \in \mathbb{R}^3$ and the velocity $v_0 = [v_{x,0}, v_{y,0}, v_{z,0}]^T \in \mathbb{R}^3$. Moreover, the setting of the leader trajectory can be set at will; only make sure that the following is satisfied: (1) v_0 is differentiable; (2) the acceleration $\widehat{v}_0$ is bounded.

(2) For the tracking control level, the technology of PID control method is used. The virtual state information of each quadrotor can be used as input data of the tracking control module, which is composed of an attitude controller and a position controller. Each quadrotor tracks the virtual state which is received from the coordination module. Finally, thrust T_i and torque τ_i are obtained as outputs.

3.1. Coordinating Control. For the cooperative control part, its advantage is that it is separated from the control part of a single quadrotor; that is to say, the design of the coordinated controller is not involved in dynamics model. The controller is set as follows:

$$\dot{\widehat{v}}_i(t) = -\lambda_1\left(\sum_{j=0}^{n} a_{ij}\left(\widehat{v}_j(t) - \widehat{v}_i(t)\right)\right)^{1-(a/b)} - \lambda_2\left(\sum_{j=0}^{n} a_{ij}\left(\widehat{v}_j(t) - \widehat{v}_i(t)\right)\right)^{1+(a/b)}, \tag{7}$$

$$\dot{\widehat{r}}_i(t) = \widehat{v}_i(t) - \lambda_3\left(\sum_{j=0}^{n} a_{ij}\left(\widehat{r}_i(t) - \widehat{r}_j(t)\right)\right)^{1-(a/b)} - \lambda_4\left(\sum_{j=0}^{n} a_{ij}\left(\widehat{r}_i(t) - \widehat{r}_j(t)\right)\right)^{1+(a/b)}, \tag{8}$$

where $\lambda_i > 0\,(i = \{1, 2, 3, 4\})$ and a is a positive even number, while b is a positive odd number, satisfying $0 < a < b$. Furthermore, when information exchanges between the ith and jth quadrotor, then $a_{ij} = 1$; otherwise $a_{ij} = 0$. After the calculation of the coordinated controller, the virtual velocity of the quadrotors reaches a fixed-time consistency, i.e., $\widehat{r}_i \longrightarrow r_0$ and $\widehat{v}_i \longrightarrow v_0$.

Although a consensus on the virtual location has been reached, the required formation shape has not yet been accomplished. In order for the quadrotors to reach a desired

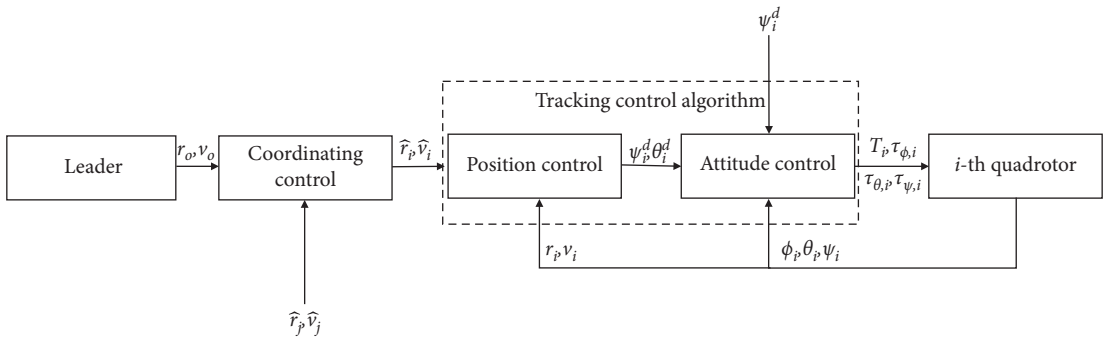

Figure 1: The diagram of hierarchical formation control.

formation pattern, a reference configuration vector σ_{ij} was introduced. According to the descriptions above, the controller (7) is rewritten:

$$\dot{\hat{r}}_i(t) = \hat{v}_i(t) - \lambda_1\left(\sum_{j=0}^{n} a_{ij}\left(\hat{r}_i(t) - \hat{r}_j(t) - \sigma_{ij}\right)\right)^{1-(a/b)} - \lambda_2\left(\sum_{j=0}^{n} a_{ij}\left(\hat{r}_i(t) - \hat{r}_j(t) - \sigma_{ij}\right)\right)^{1+(a/b)}, \tag{9}$$

where $\sigma_{ij} = \sigma_i - \sigma_j$ is formation reference configuration vector, the proposed coordinating control algorithm without the traditional symbol function sign $(\cdot)$; that is to say, equation (8) is a smooth and continuous consensus protocol, thereby effectively preventing the occurrence of tremor.

3.2. Tracking Control. In this section, in order to make the real position and real velocity converge to the virtual positon and virtual velocity, i.e., $r_i \longrightarrow \hat{r}_i$, $v_i \longrightarrow \hat{v}_i$, a position controller and an attitude controller are designed. The tracking control algorithm is based on the PID theory, and its main advantage is that it can be implemented faster and better, and it provides a basis for actual flight experiments in future research.

3.2.1. Position Controller. Using the classic PID control, the position controller u_i^p is presented:

$$u_i^p = \dot{\hat{v}}_i + k_p e(t) + k_i \int e(t)\mathrm{d}t + k_d \frac{\mathrm{d}e(t)}{\mathrm{d}t}, \quad i \in \Gamma, \tag{10}$$

where $e(t) = \hat{r}_i - r_i$ and $k_p, k_i, k_d > 0$ are PID parameters. According to the position dynamical model in (3), the position controller is presented:

$$\begin{aligned}
u_{x,i}^p &= \frac{T_i}{m_i}\left(\cos\phi_i^d \cos\psi_i^d \sin\theta_i^d + \sin\phi_i^d \sin\psi_i^d\right) - \frac{k_{x,i}}{m_i}\dot{x}_i,\\
u_{y,i}^p &= \frac{T_i}{m_i}\left(\cos\phi_i^d \sin\psi_i^d \sin\theta_i^d - \cos\psi_i^d \sin\phi_i^d\right) - \frac{k_{y,i}}{m_i}\dot{y}_i,\\
u_{z,i}^p &= \frac{T_i}{m_i}\cos\phi_i^d \cos\theta_i^d - \frac{k_{z,i}}{m_i}\dot{z}_i - g,\\
&i \in \Gamma,\\
e_1 &= \hat{r}_i - r_i,\\
e_2 &= \hat{v}_i - v_i,
\end{aligned} \tag{11}$$

and then, the position formula u_i^p is designed as follows:

$$u_i^p = \dot{\hat{v}}_i + k_1 e_1 + k_2 \int e_1 \mathrm{d}t + k_3 e_2, \quad i \in B, \tag{12}$$

where $k_1 > 0$, $k_2 > 0$, and $k_3 > 0$.

3.2.2. Attitude Controller. The desired attitudes, roll ϕ_i^d and pitch θ_i^d, of each quadrotor are obtained by the virtual inputs $u_i^p = (u_{x,i}^p, u_{y,i}^p, u_{z,i}^p)$. In addition, considering the desired yaw

angle ψ_i^d is a free variable, for more convenient analysis, it can be set as $\psi_i^d = 0$; hence,

$$\begin{aligned} T_i^d &= m_i\sqrt{\left(u_{i,x}^p\right)^2 + \left(u_{i,y}^p\right)^2 + \left(u_{i,z}^p + g\right)^2}, \\ \phi_i^d &= \arcsin\left(\frac{-m_i u_{y,i}^p}{T_i^d}\right), \\ \theta_i^d &= \arctan\left(\frac{u_{x,i}^p}{u_{z,i}^p + g}\right), \\ i &\in \Gamma. \end{aligned} \tag{13}$$

Similarly, the attitude controller $u_i^a = [u_{x,i}^a, u_{y,i}^a, u_{z,i}^a]^T \in \mathbb{R}^3$ is designed; that is,

$$u_i^a = \ddot{\Phi}_i + k_4 e_2 + k_5 \int e_2 \mathrm{d}t + k_6 \dot{e}_2, \quad i \in B, \tag{14}$$

where $\Phi_i^d = [\phi_i^d, \theta_i^d, \psi_i^d]^T$ is the desired attitude angles, and $e_2 = \Phi_i^d - \Phi_i, \dot{e}_3 = \dot{\Phi}_i^d - \dot{\Phi}_i$. Next, u_i^a in the attitude dynamic algorithm is

$$\begin{aligned} u_{x,i}^a &= \frac{1}{I_{x,i}}\left(I_{y,i} - I_{z,i}\right)\dot{\theta}_i\dot{\psi}_i + \frac{\tau_{\phi,i}^d}{I_{x,i}} - \frac{k_{\phi,i}}{I_{x,i}}\dot{\phi}_i, \\ u_{y,i}^a &= \frac{1}{I_{y,i}}\left(I_{z,i} - I_{x,i}\right)\dot{\phi}_i\dot{\psi}_i + \frac{\tau_{\theta,i}^d}{I_{y,i}} - \frac{k_{\theta,i}}{I_{y,i}}\dot{\theta}_i, \\ u_{z,i}^a &= \frac{1}{I_{z,i}}\left(I_{x,i} - I_{y,i}\right)\dot{\theta}_i\dot{\phi}_i + \frac{\tau_{\psi,i}^d}{I_{z,i}} - \frac{k_{\psi,i}}{I_{z,i}}\dot{\psi}_i, \\ i &\in \Gamma. \end{aligned} \tag{15}$$

According to the results above, the desired torque $\tau_i^d = [\tau_{\phi,i}^d, \tau_{\theta,i}^d, \tau_{\psi,i}^d]^T$ and the velocity of each quadrotor can be obtained.

4. Theoretical Proof

The stability proof of the coordinating control algorithm is given.

Theorem 1. *Suppose that the undirected communication topology $G_n = \{V, E, A\}$ for the quadrotors connected; then, the coordinating control protocol (7) can achieve consensus in fixed-time, and the settling time T satisfies*

$$T \le T_{\max}^1 = \frac{b}{2^{-(a/b)} a\lambda_1\lambda_*\left(\mathbb{L}_p\right)^{1-(a/2b)}} + \frac{b}{2^{(a/b)} n^{-(7a/6b)} a\lambda_2\lambda_*\left(\mathbb{L}_q\right)^{1+(a/2b)}}. \tag{16}$$

Proof. Define

$$\begin{aligned} \bar{\hat{v}}_i &= \hat{v}_i - \hat{v}_0, \\ e_i &= \bar{\hat{v}}_i - \frac{1}{n}\sum_{j=1}^n \bar{\hat{v}}_j. \end{aligned} \tag{17}$$

Set a Lyapunov constructor as follows:

$$V = \frac{1}{2}\sum_{i=1}^n \left(e_i^T e_i\right), \tag{18}$$

where $V \ge 0$; its time derivative can be calculated by

$$\begin{aligned} \dot{V} &= \sum_{i=1}^n e_i^T \dot{e}_i \\ &= -\lambda_1 \sum_{i=1}^n\sum_{j=1}^n a_{ij} e_i^T \left(\bar{\hat{v}}_i - \bar{\hat{v}}_j\right)^{1-(a/b)} - \lambda_2 \sum_{i=1}^n\sum_{j=1}^n a_{ij} e_i^T \left(\bar{\hat{v}}_i - \bar{\hat{v}}_j\right)^{1+(a/b)}. \end{aligned} \tag{19}$$

For the first term in $\dot{V}$,

$$
\begin{aligned}
&-\lambda_1 \sum_{i=1}^{n}\sum_{j=1}^{n} a_{ij} e_i^T \left(\bar{\hat{v}}_i - \bar{\hat{v}}_j\right)^{1-(a/b)} = -\lambda_1 \sum_{i=1}^{n}\sum_{j=1}^{n} a_{ij} e_i^T \left(e_i - e_j\right)^{1-(a/b)} \\
&= -\frac{\lambda_1}{2} \sum_{i=1}^{n}\sum_{j=1}^{n} a_{ij} e_i^T \left(e_i - e_j\right)^{1-(a/b)} - \frac{\lambda_1}{2} \sum_{j=1}^{n}\sum_{i=1}^{n} a_{ji} e_j^T \left(e_j - e_i\right)^{1-(a/b)} \\
&= -\frac{\lambda_1}{2} \sum_{i=1}^{n}\sum_{j=1}^{n} a_{ij} e_i^T \left(e_i - e_j\right)^{1-(a/b)} + \frac{\lambda_1}{2} \sum_{i=1}^{n}\sum_{j=1}^{n} a_{ij} e_j^T \left(e_i - e_j\right)^{1-(a/b)} \\
&= -\frac{\lambda_1}{2} \sum_{i=1}^{n}\sum_{j=1}^{n} a_{ij} \left\| e_i - e_j \right\|_{2-(a/b)}^{2-(a/b)}.
\end{aligned}
\tag{20}
$$

Then, in a similar way for the second term, it can be obtained that

$$
-\lambda_2 \sum_{i=1}^{n}\sum_{j=1}^{n} a_{ij} e_i^T \left(\bar{\hat{v}}_i - \bar{\hat{v}}_j\right)^{1+(a/b)} = -\frac{\lambda_2}{2} \sum_{i=1}^{n}\sum_{j=1}^{n} a_{ij} \left\| e_i - e_j \right\|_{2+(a/b)}^{2+(a/b)}.
\tag{21}
$$

Therefore, it can be obtained that

$$
\begin{aligned}
\dot{V} &= -\frac{\lambda_1}{2} \sum_{i=1}^{n}\sum_{j=1}^{n} a_{ij} \left\| e_i - e_j \right\|_{2-(a/b)}^{2-(a/b)} - \frac{\lambda_2}{2} \sum_{i=1}^{n}\sum_{j=1}^{n} a_{ij} \left\| e_i - e_j \right\|_{2+(a/b)}^{2+(a/b)} \\
&\le -\frac{\lambda_1}{2} \sum_{i=1}^{n}\sum_{j=1}^{n} a_{ij} \left\| e_i - e_j \right\|_{2}^{2-(a/b)} - \frac{\lambda_2}{2} \sum_{i=1}^{n}\sum_{j=1}^{n} a_{ij} \left\| e_i - e_j \right\|_{2}^{2+(a/b)} \\
&\le -\frac{\lambda_1}{2} \sum_{i=1}^{n}\sum_{j=1}^{n} a_{ij} \left\| e_i - e_j \right\|_{2}^{2-(a/b)} - \frac{\lambda_2}{2} \sum_{i=1}^{n}\sum_{j=1}^{n} a_{ij} n^{-(a/2b)} \left\| e_i - e_j \right\|_{2}^{2+(a/b)} \\
&= -\frac{\lambda_1}{2} \sum_{i=1}^{n}\sum_{j=1}^{n} \left(a_{ij}^{(2b/2b-a)} \left\| e_i - e_j \right\|_{2}^{2} \right)^{(2b-a/2b)} - \frac{\lambda_2}{2} n^{-(a/2b)} \sum_{i=1}^{n}\sum_{j=1}^{n} \left(a_{ij}^{(2b/2b+a)} \left\| e_i - e_j \right\|_{2}^{2} \right)^{(2b+a/2b)} \\
&\le -\frac{\lambda_1}{2} \sum_{i=1}^{n}\sum_{j=1}^{n} \left(a_{ij}^{(2b/2b-a)} \left\| e_i - e_j \right\|_{2}^{2} \right)^{(2b-a/2b)} - \frac{\lambda_2}{2} n^{-(7a/6b)} \sum_{i=1}^{n}\sum_{j=1}^{n} \left(a_{ij}^{(2b/2b+a)} \left\| e_i - e_j \right\|_{2}^{2} \right)^{(2b+a/2b)}.
\end{aligned}
\tag{22}
$$

Then, due to [16], we have

$$
\begin{aligned}
\sum_{i,j=1}^{n} a_{ij}^{(2b/2b-a)} \left\| e_i - e_j \right\|_{2}^{2} &= 2e^T \mathbb{L}_p e \ge 4\lambda_* \left(\mathbb{L}_p\right) V, \\
\sum_{i,j=1}^{n} a_{ij}^{(2b/2b+a)} \left\| e_i - e_j \right\|_{2}^{2} &= 2e^T \mathbb{L}_q e \ge 4\lambda_* \left(\mathbb{L}_q\right) V,
\end{aligned}
\tag{23}
$$

where $e = [e_1, e_2, \ldots, e_n]^T$, $\mathbb{L}_p$ and $\mathbb{L}_q$ are the Laplacians of the graphs $G(A^{(2b/2b-a)})$ and $G(A^{(2b/2b+a)})$, respectively, and $\lambda_*(\mathbb{L}_p)$ And $\lambda_*(\mathbb{L}_q)$ are the second smallest eigenvalues of $\mathbb{L}_p$ and $\mathbb{L}_q$, respectively.

Therefore, we get

$$
\begin{aligned}
\dot{V} &\le -\frac{\lambda_1}{2} \left(4\lambda_* \left(\mathbb{L}_p\right) V\right)^{(2b-a/2b)} - \frac{\lambda_2}{2} n^{-(7a/6b)} \left(4\lambda_* \left(\mathbb{L}_q\right) V\right)^{(2b+a/2b)} \\
&= -\frac{\lambda_1}{2} \left(4\lambda_* \left(\mathbb{L}_p\right)\right)^{(2b-a/2b)} V^{(2b-a/2b)} - \frac{\lambda_2}{2} n^{-(7a/6b)} \left(4\lambda_* \left(\mathbb{L}_q\right)\right)^{(2b+a/2b)} V^{(2b+a/2b)}.
\end{aligned}
\tag{24}
$$

Invoking Lemma 2, the virtual velocity consensus is achieved in a fixed time with a setting time T. Furthermore, $\hat{v}_i \longrightarrow \hat{v}_0$ when $T \le T_{\max}^1$; this completes the proof.

Next, the position consensus is considered, and the related theorem and proof are as follows. □

Theorem 2. *Suppose that the undirected communication topology $G_n = \{V, E, A\}$ for the quadrotors connected; then, the coordinating control protocol (8) can achieve consensus in fixed-time, and the settling time T satisfies*

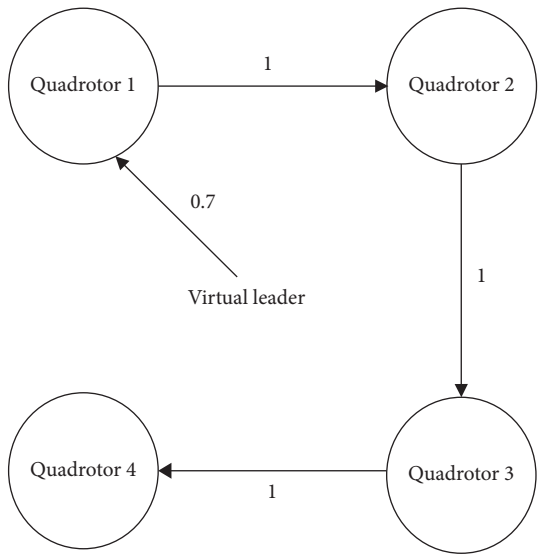

Figure 2: Communication topology and the desired formation shape.

Table 1: Parameters of control algorithms.

Parameter	Value
λ_1	3.0
λ_2	0.6
λ_3	3.5
λ_4	0.7
a	5.00
b	49.0
k_1	6
k_2	5
k_3	8
k_4	500
k_5	300
k_6	30

$$T \le T_{\max}^2 = \frac{b}{2^{-(a/b)} a\lambda_3\lambda_* \left(\mathbb{L}_p\right)^{1-(a/2b)}} + \frac{b}{2^{(a/b)} n^{-(7a/6b)} a\lambda_4\lambda_* \left(\mathbb{L}_q\right)^{1+(a/2b)}}. \tag{25}$$

Proof. Basically, it is the same as the proof of Theorem 1, so we only present the main part to avoid redundancy. Based on the virtual velocity consensus results, it can be obtained that $\hat{v}_i = \hat{v}_j = \hat{v}_0 = \dot{\hat{r}}_0$ when $T \le T_{\max}^1$. Define

$$\begin{aligned} \bar{\hat{r}}_i &= \hat{r}_i - \hat{r}_0, \\ \bar{\hat{v}}_i &= \hat{v}_i - \hat{v}_0. \end{aligned} \tag{26}$$

Hence, protocol (8) can be changed as follows:

$$\dot{\bar{\hat{r}}}_i(t) = -\lambda_3 \left(\sum_{j=0}^{n} a_{ij} \left(\bar{\hat{r}}_i(t) - \bar{\hat{r}}_j(t) \right) \right)^{1-(a/b)} - \lambda_4 \left(\sum_{j=0}^{n} a_{ij} \left(\bar{\hat{r}}_i(t) - \bar{\hat{r}}_j(t) \right) \right)^{1+(a/b)}. \tag{27}$$

Similarly, set a Lyapunov constructor

$$V = \frac{1}{2} \sum_{i=1}^{n} \left(e_i^T e_i \right). \tag{28}$$

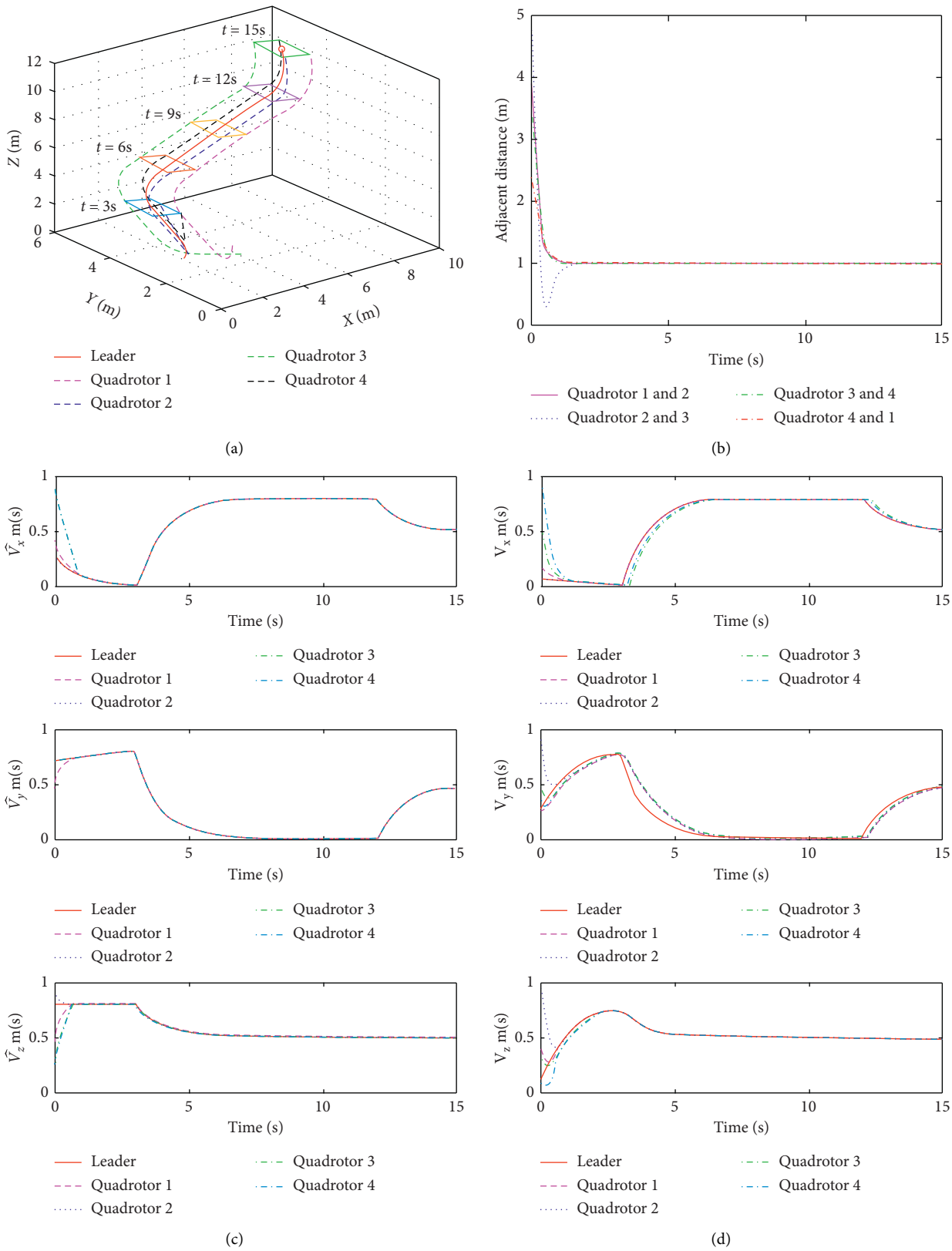

Figure 3: Continued.

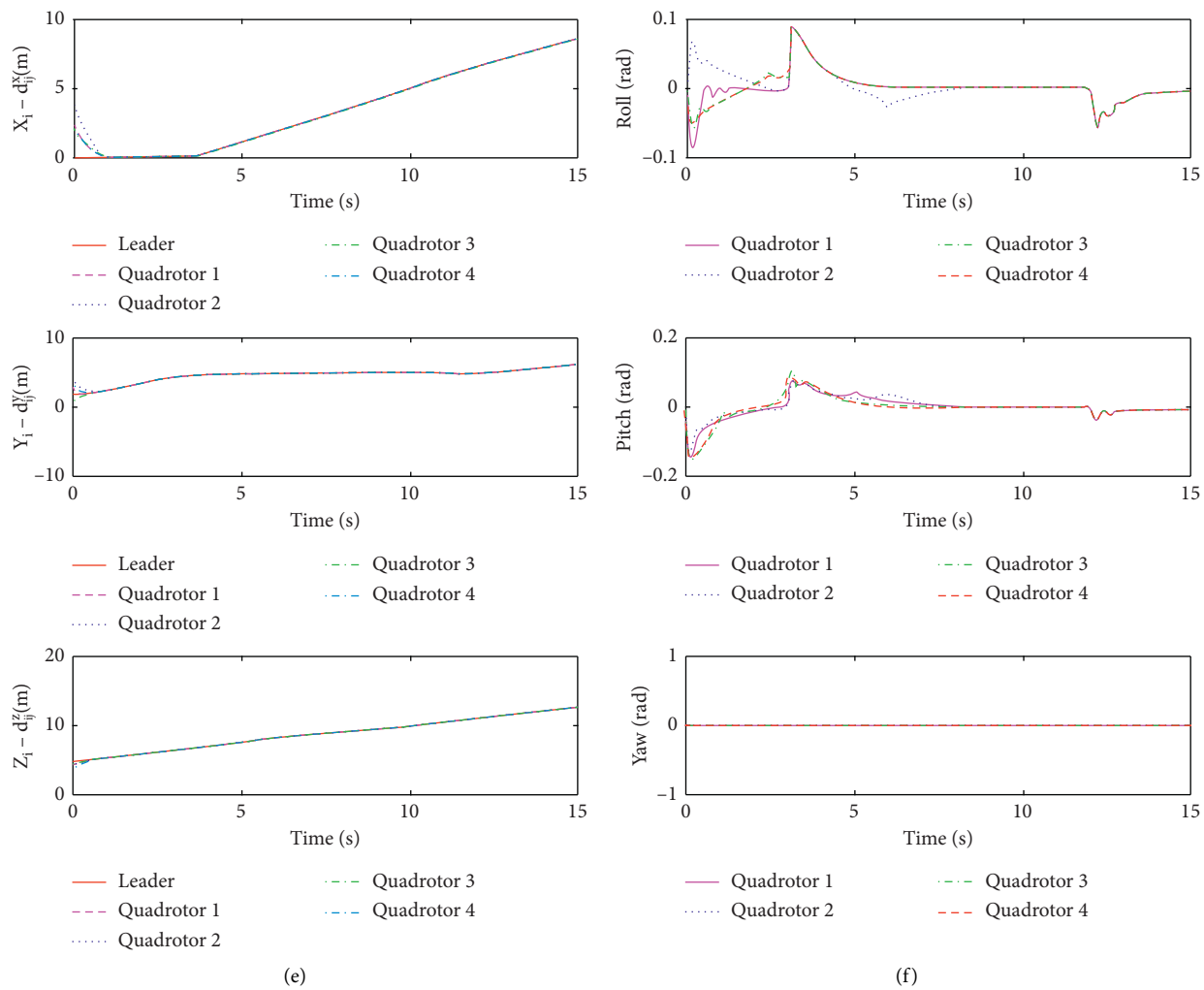

Figure 3: Simulation results. (a) The trajectory of all quadrotors in 3D space. (b) The adjacent distance between every two quadrotors. (c) The virtual velocity of all quadrotors. (d) The real velocity of all quadrotors. (e) The position curves of the leader and the quadrotors. (f) Response of attitude angles of all quadrotors.

Then, one finally obtains

$$\dot{V} \leq -\frac{\lambda_3}{2}\left(4\lambda_*\left(\mathbb{L}_p\right)\right)^{(2b-a/2b)} V^{(2b-a/2b)} - \frac{\lambda_4}{2} n^{-(7a/6b)} \left(4\lambda_*\left(\mathbb{L}_q\right)\right)^{(2b+a/2b)} V^{(2b+a/2b)}. \tag{29}$$

Thus, similar to the proof of Theorem 1, multiple quadrotors reach the fixed-time consensus within $T_{\max}^2$, which means the formation shape of multiquadrotors can be obtained in fixed time. □

5. Simulation Results

In this section, simulation experiments are used to illustrate the feasibility and superiority of the proposed fixed-time consistency control algorithm. The following content will be divided into two parts for verification of the feasibility and superiority of the control algorithm.

5.1. The Feasibility of the Algorithm. The communication topology of a five-node multiquadrotor system includes four followers and a virtual leader; the four quadrotors form a square as the desired formation shape. The leader points to quadrotor 1, which means that data can be transmitted in a directional manner and the communication method of other quadrotors is presented by the direction of the arrow as presented in Figure 2. Therefore, the weight of the edge is, respectively, presented as follows: $a_{21} = a_{31} = a_{41} = a_{51} = 1$, for each quadrotor, the moments of inertia are chosen: $I_{x,i} = 0.05, I_{y,i} = 0.05, I_{z,i} = 0.1$, the air resistance coefficients are chosen as $k_{x,i} = k_{y,i} = k_{z,i} = 0.02$, and the torque

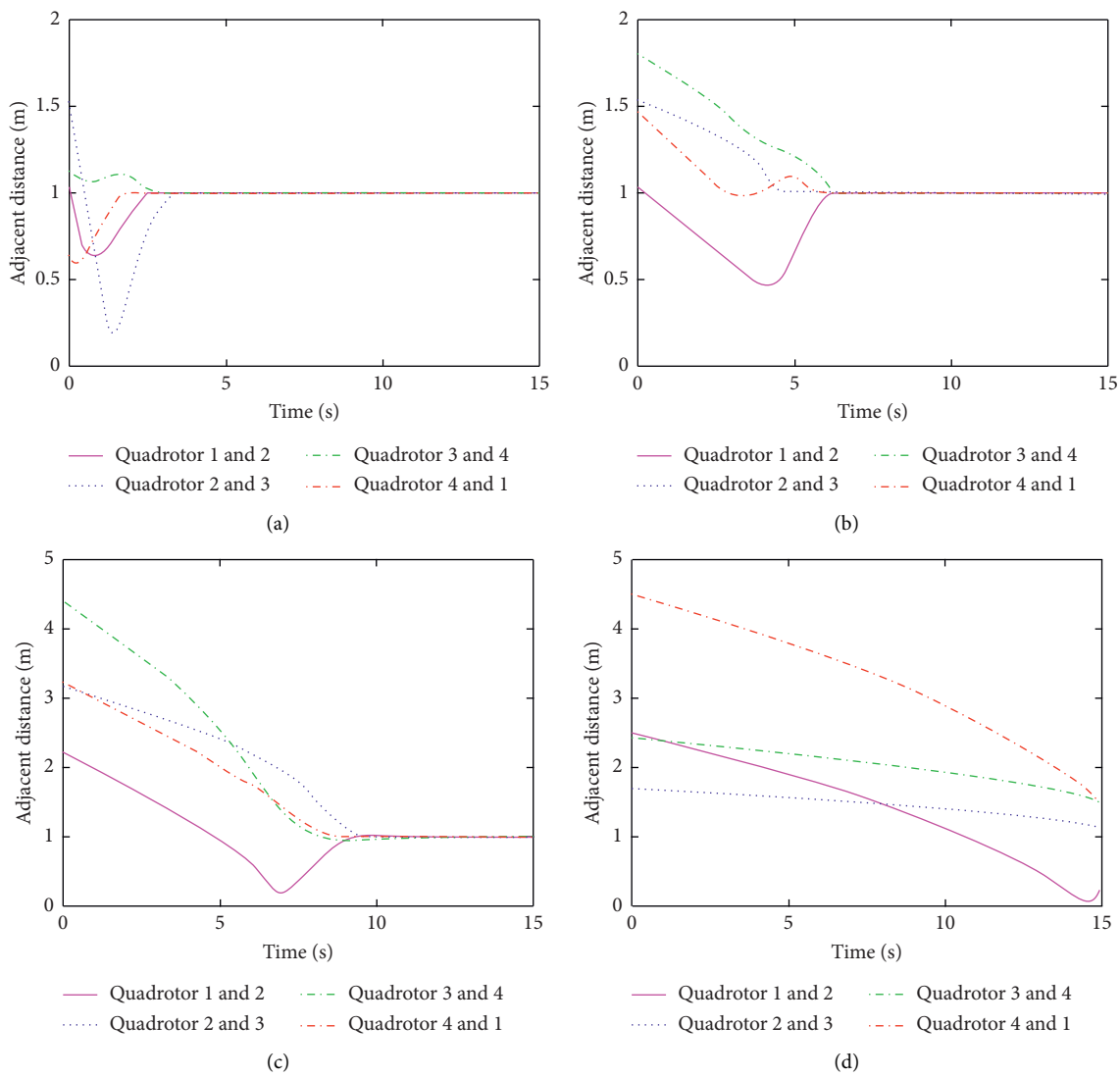

FIGURE 4: The adjacent distance between every two quadrotors under the control algorithm (34). (a) In the range of (0, 2). (b) In the range of (3, 5). (c) In the range of (5, 10). (d) In the range of (10, 20).

coefficients $k_{\phi,i} = k_{\theta,i} = k_{\psi,i} = 0.1$. In addition, the parameters of control algorithm are presented in Table 1.

Remark 1. Due to the control saturation constraints of the real quadrotors and the formation control problem, the quadrotor cannot quickly fly, parameters $\lambda_i\,(i = \{1, 2, 3, 4\})$ cannot be set too large values, and one can usually set the parameters within (0, 5]. In order to keep the better performance of fixed-time convergence and disturbance rejection, the parameters a and b are usually set to $a/b \in (0, 1)$.

In simulations, the leader's initial state information is set:

$$\begin{aligned}&\left[r_{0,x}(0), r_{0,y}(0), r_{0,z}(0), v_{0,x}(0), v_{0,y}(0), v_{z,0}(0)\right]^T \\ &\quad = [0.3, 1.5, 2.55, 2.78, 0.80, 0.90]^T.\end{aligned} \tag{30}$$

The initial acceleration for the leader is

$$a_0(t) = \begin{cases} [0, 1, 1]^T - v_0(t), & 0 \le t < 3, \\ [0.9, 0, 0.6]^T - v_0(t), & 3 \le t < 12, \\ [0.6, 0.6, 0.6]^T - v_0(t), & 12 \le t \le 15. \end{cases} \tag{31}$$

Then, through curve fitting, the leader's trajectory curve can be approximated by the following function:

$$f(x, y) = 5.798 - 0.2985\,\sin(0.7926\pi(xy)) + 10.56e^{-(3.413y)^2}. \tag{32}$$

Next, one will choose the initial conditions of four quadrotors as follows:

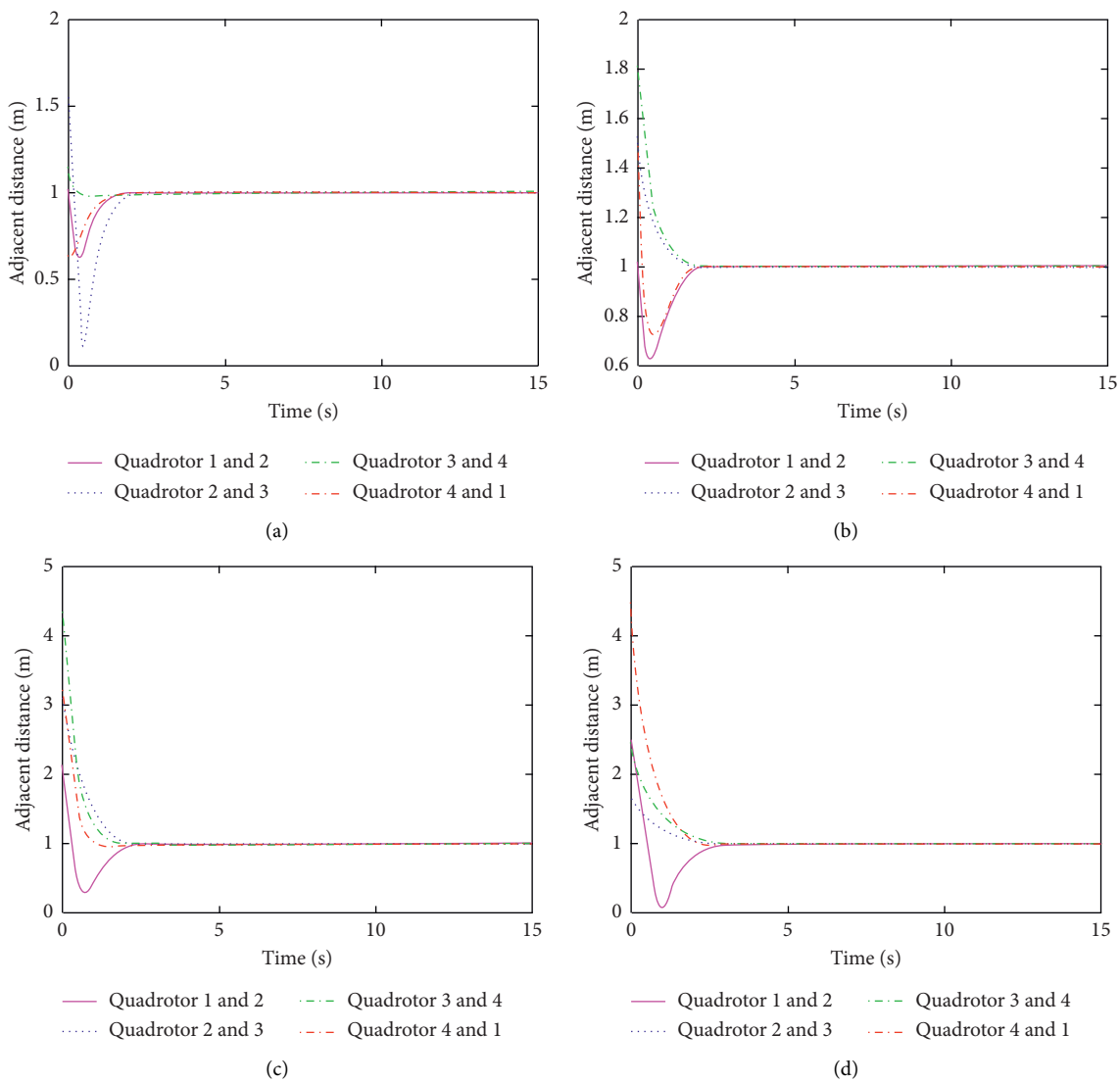

Figure 5: The adjacent distance between every two quadrotors under the control algorithm (9). (a) In the range of (0, 2). (b) In the range of (3, 5). (c) In the range of (5, 10). (d) In the range of (10, 20).

Table 2: Comparison results with two control algorithms.

	$t_{(0,2)}$	$t_{(3,5)}$	$t_{(5,10)}$	$t_{(10,20)}$
Control algorithm (34)	3.39	6.49	9.85	>15
Control algorithm (9)	2.53	2.51	2.54	2.79
Performance improvement (%)	25.4	61.3	74.2	>81

$$\begin{aligned}
\left[r_{1,x}(0), r_{1,y}(0), r_{1,z}(0), v_{1,x}(0), v_{1,y}(0), v_{1,z}(0)\right]^T &= [3.20, 2.10, 2.50, 0.55, 0.56, 0.47]^T, \\
\left[r_{2,x}(0), r_{2,y}(0), r_{2,z}(0), v_{2,x}(0), v_{2,y}(0), v_{2,z}(0)\right]^T &= [3.30, 5.10, 1.78, 0.25, 0.77, 0.95]^T, \\
\left[r_{3,x}(0), r_{3,y}(0), r_{3,z}(0), v_{3,x}(0), v_{3,y}(0), v_{3,z}(0)\right]^T &= [1.70, 0.50, 1.77, 0.88, 0.69, 0.27]^T, \\
\left[r_{4,x}(0), r_{4,y}(0), r_{4,z}(0), v_{4,x}(0), v_{4,y}(0), v_{4,z}(0)\right]^T &= [2.70, 3.00, 1.85, 0.65, 0.79, 0.28]^T.
\end{aligned} \tag{33}$$

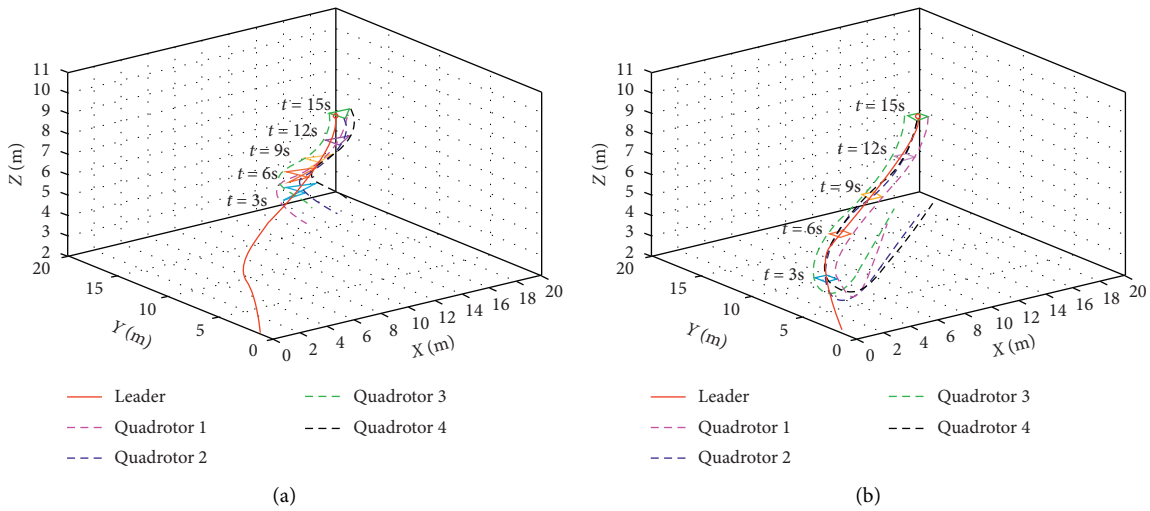

Figure 6: The flight trajectory of all quadrotors in the range of (10, 20). (a) Under the control algorithm (34). (b) Under the control algorithm (9).

Based on the proposed control architecture, simulation outcomes are shown in Figure 3. The response of position trajectories of all quadrotor in 3D space is shown in Figure 3(a), and the red curve denotes the trajectory of the virtual leader; it can be seen that the desired formation has been formed within 3 seconds; then the four quadrotors followed the leader to fly in the desired square formation. Figure 3(b) shows the adjacent distance between two quadrotors converges to 1.0 m; as can be seen from the figure, the convergence of the four quadrotor is extremely fast. Figures 3(c) and 3(d) represent the virtual velocity curve and real velocity curve of each quadrotor. In the hierarchical formation control framework, the virtual velocity can be obtained by the coordinating control algorithm and making the virtual velocity reach a fixed-time consistency; from Figure 3(c), one can see that the virtual velocity of quadrotors reaches consistency within 2 seconds. Meanwhile, the real velocity can track the virtual velocity by the tracking control algorithm; therefore, the real velocity eventually reaches consistency as shown in Figure 3(d). Furthermore, at the 3rd and 12th seconds, the acceleration of the leader changes, and the velocity of the quadrotor quickly reaches consensus. Figure 3(e) shows the position of all quadrotors which well reflects the position consensus. The attitude angles of each quadrotor aircraft are given in Figure 3(f), from which one can see that the sudden change of the leader's trajectory will slightly affect the pitch angle and roll angle but overall it maintains a good convergence.

5.2. The Superiority of the Algorithm. In order to verify the superiority of the proposed fixed-time hierarchical control algorithm, that is, the convergence time of the quadrotor system is not affected by its initial state, the comparative simulations were conducted.

The comparative controller is a finite-time consistency control protocol; refer to [23]; the controller is selected as follows:

$$\begin{aligned}\dot{\hat{v}}_i(t) &= \gamma_1 \operatorname{sig}^{\beta_1}\left(\sum_{j=0}^{n} a_{ij}\left(\hat{v}_j(t) - \hat{v}_i(t)\right)\right),\\ \dot{\hat{r}}_i(t) &= \hat{v}_i(t) - \gamma_2 \operatorname{sig}^{\beta_2}\left(\sum_{j=0}^{n} a_{ij}\left(\hat{r}_i(t) - \hat{r}_j(t) - \sigma_{ij}\right)\right),\end{aligned} \tag{34}$$

where $\gamma_1 > 0$, $\gamma_2 > 0$, $\beta_1 \in (0,1)$, and $\beta_2 \in (0,1)$. During simulations, the parameters of the controller (34) are all optimal values.

In the simulations, the initial position of the leader quadrotor remains unchanged, which is set

$$\begin{aligned}&\left[r_{0,x}(0), r_{0,y}(0), r_{0,z}(0), v_{0,x}(0), v_{0,y}(0), v_{z,0}(0)\right]^T\\ &\quad = [0.2, 1.6, 2.0, 0.50, 0.50, 0.50]^T.\end{aligned} \tag{35}$$

Next, four sets of initial positions are given for the four follower quadrotors; in order to conform to the reality, the position coordinates in the Z-axis direction are set to $r_{i,z}(0) = 2$. Meanwhile, the initial positions of the quadrotors in the X-axis and Y-axis directions are in the four ranges (0, 2), (3, 5), (5, 10), and (10, 20), respectively. As a special case, the initial positions in the range of (10, 20) are given below:

$$\begin{aligned}\left[r_{1,x}(0), r_{1,y}(0), r_{1,z}(0)\right]^T &= [15.0, 16.3, 2.0]^T,\\ \left[r_{2,x}(0), r_{2,y}(0), r_{2,z}(0)\right]^T &= [17.5, 16.2, 2.0]^T,\\ \left[r_{3,x}(0), r_{3,y}(0), r_{3,z}(0)\right]^T &= [16.9, 18.2, 2.0]^T,\\ \left[r_{4,x}(0), r_{4,y}(0), r_{4,z}(0)\right]^T &= [19.3, 17.6, 2.0]^T.\end{aligned} \tag{36}$$

In addition, the initial state of this simulation takes the position as an example, so the initial velocities of the four quadrotors are set as $[v_{i,x}(0), v_{i,y}(0), v_{i,z}(0)]^T = [0.5, 0.5, 0.5]^T$.

Based on the above analysis and data, the simulation results are shown in Figures 4–6. Figure 4 shows the

response curves of the distance between the quadrotors in the three-dimensional space under the control algorithm (34), from which it can be seen that all the quadrotors converge to the desired formation shape and move along the desired trajectory within 15 seconds in Figures 4(a)–4(c), except for Figure 4(d). Meanwhile, in the range of (0, 2), (3, 5), (5, 10), the convergence time of the four quadrotors is 3.39 s, 6.49 s, and 9.85 s, respectively. It can be seen that, under the control algorithm (34), as the distance between the follower quadrotors and the leader increases, the convergence time also increases. However, as can be seen from Figure 5, under the control algorithm (9), the quadrotors reach the convergence faster, and the convergence time is not affected by the initial position. Specifically, the comparison results are shown in Table 2. It is obvious from Table 2 that, compared to the control algorithm (34), the control algorithm (9) converges faster under the same conditions and, no matter how the initial position changes, the convergence time remains basically the same. Furthermore, Figure 6 shows the flight trajectory of all quadrotors in the range of (10, 20), and the flight trajectory well shows the superiority of the control algorithm (9).

6. Conclusion

A hierarchical formation control structure which can solve the problem of multiquadrotor control has been developed through the previous discussion. First, this new kind of formation control structure is composed of a coordinating control part and a tracking control part. Based on the fixed-time consensus methods and PID methods, respectively, a coordinating control algorithm and a tracking control algorithm are given. Second, we have proved the convergence of the coordinating control algorithm in detail and illustrated the feasibility of the algorithm. Third, the proposed control algorithm has a good reference value in practical applications and can be used in actual flight. Finally, the aforementioned simulation results have elaborated the feasibility and superiority of hierarchical formation control structure.

Data Availability

The simulation data used to support the findings of this study have not been made available because the data also form part of an ongoing study.

Conflicts of Interest

The authors declare that they have no conflicts of interest.

Acknowledgments

This work was supported in part by the New Talent Plan Project of Zhejiang Province (Zhejiang Provincial Science and Technology Innovation Activity Plan for University Students) under Grant 2020R407075 and in part by the Zhejiang Provincial Public Welfare Technology Foundation of China under Grant LGF19F030003.

References

[1] M. Aljehani and M. Inoue, "Performance evaluation of multi-UAV system in post-disaster application: validated by HITL simulator," *IEEE Access*, vol. 7, pp. 64386–64400, 2019.

[2] B. Tian, Y. Ma, and Q. Zong, "A continuous finite-time output feedback control scheme and its application in quadrotor UAVs," *IEEE Access*, vol. 6, pp. 19807–19813, 2018.

[3] Y. Li, J. Yang, and K. Zhang, "Distributed finite-Time cooperative control for quadrotor formation," *IEEE Access*, vol. 7, pp. 66753–66763, 2019.

[4] Y. Cao, W. Ren, and Z. Meng, "Decentralized finite-time sliding mode estimators with applications to formation tracking," in *Proceedings of American Control Conference, Marriott Waterfront*, pp. 4610–4615, Baltlmore, MD, USA, June 2010.

[5] M. Saska, T. Baca, J. Thomas et al., "System for deployment of groups of unmanned micro aerial vehicles in GPS-denied environments using onboard visual relative localization," *Autonomous Robots*, vol. 41, no. 4, pp. 919–944, 2017.

[6] X. Zhang, Y. Fang, B. Li, and J. Wang, "Visual servoing of nonholonomic mobile robots with uncalibrated camera-to-robot parameters," *IEEE Transactions on Industrial Electronics*, vol. 64, no. 1, pp. 390–400, 2017.

[7] H. Liu, W. X. Ke, and H. Y. Zhu, "A novel backstepping method for the three-dimensional multi-UAVs formation control," in *Proceedings of IEEE International Conference on Mechatronics and Automation*, pp. 923–928, Seattle, WA, USA, May 2015.

[8] J. Shin, S. Kim, and J. Suk, "Development of robust flocking control law for multiple UAVs using behavioral decentralized method," *Journal of the Korean Society for Aeronautical & Space Sciences*, vol. 43, no. 10, pp. 859–867, 2015.

[9] C. Da, J. Sun, and S. Wu, "UAVs formation flight control based on behavior and virtual structure," in *Proceedings of Asian Simulation Conference*, pp. 429–438, Shanghai, China, October 2012.

[10] Q. Lu, Q. L. Han, and X. Xie, "A finite-time motion control strategy for odor source localization," *IEEE Transactions on Industrial Electronics*, vol. 61, no. 10, pp. 5419–5430, 2014.

[11] Q. Lu, Q.-L. Han, B. Zhang, D. Liu, and S. Liu, "Cooperative control of mobile sensor networks for environmental monitoring: an event-triggered finite-time control scheme," *IEEE Transactions on Cybernetics*, vol. 47, no. 12, pp. 4134–4147, 2017.

[12] S. P. Bhat and D. S. Bernstein, "Finite-time stability of homogeneous systems," in *Proceedings of the 1997 American Control Conference (Cat. No.97CH36041)*, Albuquerque, NM, USA, June 1997.

[13] S. Li, M. Zhou, and X. Yu, "Design and implementation of terminal sliding mode control method for PMSM speed regulation system," *IEEE Transactions on Industrial Informatics*, vol. 9, no. 4, pp. 1879–1891, 2013.

[14] H. Du, J. Zhang, and W. Zhu, "Finite-time consensus control for a group of quadrotor aircraft," in *Proceedings of Chinese Automation Congress*, pp. 1531–1536, Jinan, China, October 2017.

[15] A. Polyakov, "Nonlinear feedback design for fixed-time stabilization of linear control systems," *IEEE Transactions on Automatic Control*, vol. 57, no. 8, pp. 2106–2110, 2012.

[16] B. Ning, Q.-L. Han, and Z. Zuo, "Distributed optimization for multiagent systems: an edge-based fixed-time consensus approach," *IEEE Transactions on Cybernetics*, vol. 49, no. 1, pp. 122–132, 2019.

[17] Y. Zhang, L. Zeng, Y. Li, and Q. Liu, "Multi-robot formation control using leader-follower for MANET," in *Proceedings of the 2009 IEEE International Conference on Robotics and Biomimetics (ROBIO)*, pp. 337–342, Guilin, China, December 2009.

[18] B. Jiang, Q. Hu, and M. I. Friswell, "Fixed-time rendezvous control of spacecraft with a tumbling target under loss of actuator effectiveness," *IEEE Transactions on Aerospace and Electronic Systems*, vol. 52, no. 4, pp. 1576–1586, 2016.

[19] W. Deng and J. Yao, "Extended-state-observer-based adaptive control of electrohydraulic servomechanisms without velocity measurement," *IEEE/ASME Transactions on Mechatronics*, vol. 25, no. 3, pp. 1151–1161, June 2020.

[20] W. Deng, J. Yao, Y. Wang, X. Yang, and J. Chen, "Output feedback backstepping control of hydraulic actuators with valve dynamics compensation," *Mechanical Systems and Signal Processing*, vol. 158, p. 2021.

[21] S. Li and X. Wang, "Finite-time consensus and collision avoidance control algorithms for multiple AUVs," *Automatica*, vol. 49, no. 11, pp. 3359–3367, 2013.

[22] H. Du, W. Zhu, G. Wen, Z. Duan, and J. Lü, "Distributed formation control of multiple quadrotor aircraft based on nonsmooth consensus algorithms," *IEEE Transactions on Cybernetics*, vol. 49, no. 1, pp. 342–353, 2019.

[23] D. Shen and Q. Lu, "Hierarchical formation control with applications to multi-quadrotor systems," *IEEE Access*, vol. 7, pp. 130599–130609, 2019.